IEEE Access
Multidisciplinary | Rapid Review | Open Access Journal

Received July 3, 2021, accepted July 24, 2021, date of publication July 28, 2021, date of current version August 5, 2021.

Digital Object Identifier 10.1109/ACCESS.2021.3100857

Deep Learning-Aided Sensorless Control Approach for PV Converters in DC Nanogrids

ALPER NABI AKPOLAT, (Member, IEEE), ERKAN DURSUN, (Member, IEEE), AND AHMET EMIN KUZUCUOĞLU, (Member, IEEE)
Department of Electrical-Electronics Engineering, Marmara University, 34722 Istanbul, Turkey
Corresponding author: Alper Nabi Akpolat (alper.nabi@marmara.edu.tr)

ABSTRACT In a microgrid, photovoltaic (PV) systems are broadly preferred with energy storage systems (ESSs) that form small-sized direct current (DC) microgrids. They are also termed local grids i.e., DC nanogrids, which feed the local consumers to some extent in the next decades. Therefore, ESSs enable the DC nanogrids more flexible and stable by preserving the intermittent nature of renewables. Yet still, feeding local consumers smoothly with PV-battery-based systems is exceedingly a considerable theme. In this context, proper control of power electronics converters as the main carrier of the system is essential. Besides, the rise of PV applications challenges possible issues upon integrating the conventional grid. Emerging possible issues in stability, reliability, efficiency and the ways of dealing with them have been developing day by day. Thus, it is inevitable that innovative methods will be put into practice. To achieve this goal, the deep learning aided-sensorless control approach is adopted. To validate the proposed control method, the training phase is presented elaborately with the help of the experimental setup of a DC nanogrid. From the obtained results, it is concluded that the deep learning-based approach reaches very small error values, captures the system dynamics successfully, enables a flexible structure with tunable hyper-parameters, and allows the possibility to apply practically.

INDEX TERMS Deep neural network (DNN), sensorless control, deep supervised learning, photovoltaics, power electronic converters, DC microgrid, DC nanogrid.

I. INTRODUCTION

The development of renewable-based distributed generation (DG) systems such as solar, wind, and biomass, etc., has become more prevalent year by year. Especially, DG is a crucial enabler where the consumer points are far away from the central power plants. Thus, DG-based power systems are broadly preferred in direct current (DC) or alternative current (AC) microgrid applications. A microgrid is a small-scale power grid that supplies energy to the local consumers and improves flexibility [1]. Compared to DC microgrids, AC microgrids have some disadvantages such as lower efficiency, higher implementation cost, more complicated control, skin effect issue, frequency synchronization, and lower reliability [2], [3], thus DC microgrids are implemented commonly due to having intermittent DC output of DGs [4]–[6]. Microgrids can be either connected to the main grid or operate autonomously according to voltage type in the point of common coupling (PCC) [7], [8].

The associate editor coordinating the review of this manuscript and approving it for publication was Shadi Alawneh.

With regards to the two main resources such as wind and solar energy for high penetration of renewable energy-based DG units, the wind character can show nonsteady-state condition and be limited; however, the harvesting of solar energy has easily accessible and widely available energy resource compared to the wind energy. Thus, solar energy is a suitable technology for both small DG structured power applications [9]. As an effective way to the DG, photovoltaic (PV) systems have been attracting considerable interest due to easy attainability and high efficiency in DC microgrids as well. As a result of the rapid development of commercially mature PV systems, widespread applications of small-sized PV grids has been emerging as nanogrid-term which is categorized from 1.5 kW up to 5.0 kW [10]. These small-sized grids allow for the incorporation of developmental activities such as night lighting, irrigation, residential appliances, remote areas, electric vehicles, military, etc. [11].

In other words, a DC nanogrid is designed to be a reliable deliverer that can dispatch power from DGs to the local loads. Apart from being smaller size than microgrids, nanogrids are localized i.e., more customer-centric, more viable, and

easier to establish. They also can form the microgrid structure by interconnecting each other [12]. As DC nanogrids can be affected adversely by the unbalanced nature of renewables, they are operated with energy storage systems (ESSs) to mitigate the generated power and ensure uninterruptible to the critical loads [3], [13]. Power electronic converters with optimal design and proper control are deployed as a backbone of DC microgrids and also nanogrids as well, as they are known to be the most vulnerable parts in terms of reliability in these systems. [14]–[16]. Thereby, the optimal selection and proper control of power electronic converters have a crucial duty in dispatching smooth power to the loads for sustainability. Due to the rapid advancement of control theory, many advanced control and optimization algorithms have been carried out [7]. Traditional control approaches depending on the detailed parameters of the system model can expose various challenges under harsh disturbances. To this end, non-model based approaches such as model predictive controller (MPC) [17], artificial neural networks (ANNs) [18], and fuzzy logic [19], a neural network supported MPC design [20] methodologies are presented for the robust system operations, which do not need any system model but also have been observed to outperform with satisfying results. In this context, a great number of AI-based smarter aspects with artificial and deep neural networks are utilized for better performance such as control of DC-DC converter using ANNs [21] for providing stable output voltage. Similarly, [5] introduces ANN-based method to reduce the number of implemented sensors and control power converters with lower attenuation at DC bus. Furthermore, ANNs are broadly adopted in fault diagnosis [22], failure and lifetime prediction of power devices [14], long-term performance analysis for power electronic converters [23], detecting and mitigation of cyber-attacks for DC microgrids [24], optimal energy scheduling for microgrids [25] and maximum power point tracking (MPPT) techniques for PV systems [26].

One such control system currently popular in this field of research is the artificial intelligence (AI)-based deep neural network (DNN) structure which is an improved extension of ANNs. Due to these advantages, in [27], a deep convolutional neural network (CNN) structure is presented for PV power forecasting and a non-intrusive load monitoring is proposed via deep learning for residential microgrids [28]. For instance, [29] achieves voltage stabilization of the DC-DC converters with low ripples via the deep reinforcement learning technique. Additionally, short-term load forecasting for sustainable management [30] and intelligent load forecasting for energy companies [31] are presented via DNNs. With the aim of being inspired by the human brain structure, it overcomes optimal power allocation issues for islanded microgrids, which is developed through DNNs [32].

As seen in the state of the art, a promising solution to relieve the drawbacks is to use a deep learning-aided system. To provide a more reliable structure by reducing a sensor in the control layer and tackle the regression problem successfully, stages in the training and analysis process of accurate estimation, the proposed control approach is dealt with DNN which is a sub-set of AI technique, is an ideal technique. As mentioned before, the sensorless control approaches are such applications that reduce the use of sensors in the control layer of power electronic converters, which greatly enhances reliability. In this context, the proposed sensorless control approach is applied to PV-Battery-based DC nanogrid structure by forecasting sensor data through a deep learning method in the control layer. In other words, this paper proves how DNNs can help to solve regression estimation problems and reduce the number of sensors in the control layer of the power converters.

Briefly, the main contributions of the study can be summarized as the proposal of the following points:

- Proper estimation of sensor data utilized in the control layer does not only solve the regression problem but also enhances the reliability of the general system as a consequence of removing the sensor without being needed it. Thereby, the communication delay of the removed sensor is ignored, which makes the system faster.
- Since the current sensors are more vulnerable than voltage sensors in case of any sensor failure in DC system measurements, it is crucial to pay attention to imitate such a necessary output as current sensor data that has a dynamic nonlinear relationship with inputs (solar irradiance, temperature, and voltage).
- Unlike less-developed structures such ANNs, as a big dataset is not required for the training process, a supervised learning-based DNN structure can enable the exploitation of short-term forecasting hourly, daily, or weekly with few data, very small error rates, and non-delay when compared to the state of the art.
- Whilst training process, a great deal of training is executed and their results are obtained to distinguish the effect of the hyper-parameters of the DNNs.

To cover the discussed themes, the rest of this paper is organized as follows. Section II elucidates the general system description such as a physical structure of PV-Battery-based topology and the control structure of PV conversion system in the DC nanogrid structure. Section III describes the deep learning design and deployment of the DNN-based sensorless control approach is explained step by step. In Section IV, obtained numerical results are presented. Besides, the discussions are stated in Section V. Finally, the conclusion and future work remarks are clarified in Section VI.

II. GENERAL SYSTEM DESCRIPTION

A. PHYSICAL STRUCTURE OF PV-BATTERY-BASED DC NANOGRID

The PV-Battery-based DC Nanogrid comprises of a PV array as DG and battery bank as energy storage system (ESS), power electronics, filters, AC load, and grid side, which is shown in Fig. 1. Whereas the PV array is the main source, the ESS is considered as an auxiliary source. The power scale of the discussed system meets the conventional DC nanogrid structure.

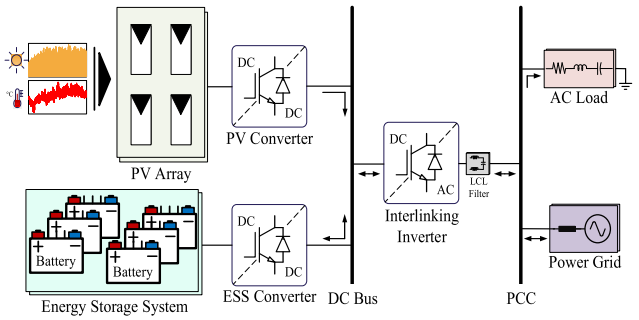

FIGURE 1. Overview of proposed PV-Battery based DC nanogrid.

As depicted, the PV array is connected to a DC bus with the help of a unidirectional DC-DC converter and maximum power point tracking (MPPT) controller. Also, the ESS is linked to the same DC-bus through a bidirectional DC-DC buck-boost converter. This topology i.e., DC nanogrid assure supplying the AC loads continuously with the proper operation of a DC-AC interlinking inverter. Since the PV array is considered as the main power source, proper operation of this conversion system is crucial for smooth power flow once any demand occurs.

The nanogrid structure in Fig. 1 represents an installed real-experimental setup system. In this nanogrid structure, the rated power of the PV array is 1 kW. As mentioned, a Perturb and Observe (P&O)-based MPPT algorithm is implemented for the proper operation of the PV conversion system in addition to the PV converter's controller. A roof-mounted PV array is preferred to utilize meteorological variables efficiently without any shading. Furthermore, a weather station is established to obtain the weather variables near the PV array on the rooftop of the faculty building. Regarding the energy storage system, six pieces of Lead-Acid battery are placed to act as a complementary power source, enhance the stability, and also alleviate the intermittent nature of physical conditions of renewables. When the PV array supplies the AC loads as a primary power source, the ESS stores unused power generated from the PV array too. The bidirectional DC-AC converter is an essential interlinking inverter that participates in system operation and feeds the loads as well. To provide smooth power to the load side and reduce the high-frequency current harmonics, an LCL filter is attached on the load side of the system towards the grid side.

The main parameters of the PV array and also other parts of the system regarding ESS, power converters, and grid are listed in Table 1. As can be seen from Table 1, the switching frequency (f_s) is attained as 10 kHz for power electronic converters. The operation of the system with these features in Table 1 is deployed and performed to procure the training data for the DNN structure to be designed.

B. CONTROL STRUCTURE OF PV ENERGY CONVERSION SYSTEM

Small-scale PV systems are broadly preferred with two-stage single-phase configuration till 30 kW rated power values [34].

TABLE 1. System parameters (See fig. 1).

VARIABLE	DESCRIPTION	VALUE
	PV ARRAY PARAMETERS	
P_{PV}	PV Array Rated Power	1 kW
V_{OC}	Open Circuit Voltage	36.3 V
I_{SC}	Short Circuit Current	34.83 A
Ns, Np	Nb of Series and Parallel Panels	2, 2
η	Module Efficiency [33]	15.40 %
	ENERGY STORAGE SYSTEM PARAMETERS	
ESS	Battery Type	Lead-Acid
V_{nom}	Nominal Voltage	24 V
Q	Nominal Capacity	600 Ah
R_{in}	Internal Resistance	3.4 mΩ
$V_{cut\text{-}off}$	Cut-off Voltage	18 V
V_{ch}	Fully Charged Voltage	27.8 V
	POWER CONVERTERS AND GRID PARAMETERS	
f_s	Switching Frequency	10 kHz
L	Boost Converter Inductor	1.5 mH
C_{PV}	PV-Side Capacitor	1000 µF
C_{DC}	DC-Bus Capacitor	1800 µF
L_f, L_G, C_f	LCL Filter	1.203 mH, *9.24* µH, *8.220* µF
V_{DC}	DC-Bus Voltage	370 V
V_G	Grid voltage (RMS)	220 V
ω	Grid nominal frequency	2π50 rad/s (50 Hz)

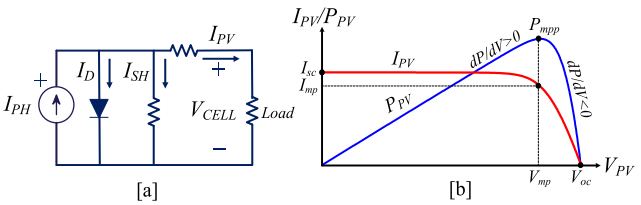

FIGURE 2. [a] Conventional equivalent circuit of PV panel (single diode model) and [b] characteristic curves.

Routine operation of power converters does not only utilize traditional multiple feedback loops with the help of proportional-integral-differential (PID) controllers but also pulse width modulation (PWM) is indispensable [35]. As a result of the PWM signal PV converter is triggered through the duty cycle (d). A proper controller is a key element in accomplishing a well-operated system [36]. As seen in Fig. 2, to extract much more power as possible and track maximum power point (MPP), a cascaded-PI reference voltage current control cascade control mechanism is activated by the P&O-based MPPT algorithm. Since obtaining the MPP from the PV array is purposed, the MPPT part requires measured voltage (V_{PV}) and current (I_{PV}) data and then adjusts the reference PV voltage (V_{PVref}) to harvest available power close to the MPP at any condition. The target of the MPPT controller is to send a PWM signal sensing the difference

between V_{PV} and I_{PV}. To this end, obtained maximum power from the PV array to the DC bus is ensured conveniently. The relationship between input and output voltage as follows:

$$d = \frac{(V_{DC} - V_{PV})}{V_{DC}}. \tag{1}$$

Upon designing the boost converter structure, the components' values should be selected properly. The boost converter inductor (L) is a function of V_{PV}, d, f_s, and lastly inductor ripple current ΔI_L as follows [37]:

$$L \geq \frac{V_{PV} d}{\Delta I_L f_s}, \tag{2}$$

Keeping a high value of I_L may cause electromagnetic interference sensitivity, otherwise taking a low value may result in unstable operation as well [38]. Thus, ΔI_L is supposed to be as 30% of I_L, i.e., between 20% and 40%. Similarly, the boost converter DC-bus capacitor (C_{DC}) is stated as:

$$C_{DC} \geq \frac{(P_{PV}/V_{DC})d}{\Delta V_{DC} f_s}, \tag{3}$$

where, P_{PV} is PV power at DC-bus, ΔV_{DC} is ripple voltage can be considered from 1% to 5% of the nominal value of V_{DC} [39].

One of the most widespread MPPT algorithms, i.e., the used P&O technique examines the change in power at the voltage-power characteristic curve of the PV panel as seen in Fig. 2 (b). If the change of power ΔP_{PVref} versus the change of voltage ΔV_{PVref} i.e., the slope of the curve (dP_{PVref}/dV_{PVref}) is higher than zero, tracking on the left side of the MPP can be deduced from that the actual power value, otherwise, dP_{PVref}/dV_{PVref} is lower than zero, actual power value wanders on the right side of the MPP, and P_{MPP} reaches at the MPP [3].

$$P_{PVref} = \begin{cases} \text{on the left side}, & \text{if } dP_{PVref}/dP_{PVref} > 0 \\ \text{on the MPP i.e.,} P_{MPP}, & \text{if } dP_{PVref}/dP_{PVref} = 0 \\ \text{on the right side}, & \text{if } dP_{PVref}/dP_{PVref} < 0 \end{cases} \tag{4}$$

or

$$\left.\frac{dP_{PVref}}{dV_{PVref}}\right|_{P_{PVref}=P_{MPP}} = 0\,. \tag{5}$$

Before proceeding, it is helpful to mention acquiring the necessary transfer function between transfer V_{PV} and d, which is constructed through the small-signal model as:

$$\frac{V_{PV}(s)}{d(s)} = \frac{\frac{-V_{DC}}{LC_{PV}}}{s^2 + \frac{s}{R_{PV}C_{PV}} + \frac{1}{LC_{PV}}}, \tag{6}$$

where, R_{PV} is the resistance of the PV array corresponds to V_{PV}/I_{PV}, which is the output resistance of the PV array. Regarding the implemented control strategy with cascaded-PI control, Fig. 3 depicts the configured controller scheme for

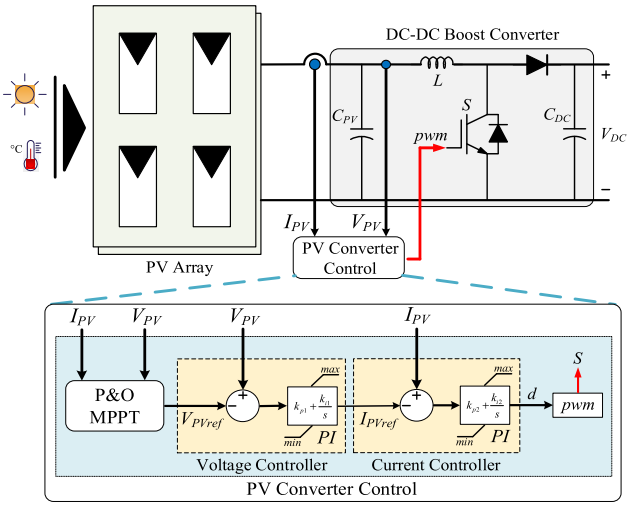

FIGURE 3. Traditional control strategy with cascaded-PI control for PV side.

a two-stage single-phase PV system. The reference current is expressed as

$$I_{PVref} = \left(k_{p1} + \frac{k_{i1}}{s}\right)(V_{PV} - V_{PVref}). \tag{7}$$

Furthermore, it is again worth mentioning that the ESS acts an important role in enhancing the system's stability, as it reduces the negative effects of the unstable nature of renewables [3]. Besides, the aim of the ESS bidirectional DC-DC buck-boost converter is to provide the stored power to the load side permanently in case of no generation from the PV side in boost mode and charge the batteries once the demand requires less than the generation in buck mode. In other words, whereas the buck mode of the converter leads to charging, the boost mode of the converter corresponds to discharging of the batteries.

Additionally, the bidirectional DC-AC inverter supplies generated power to the load side adjusting the DC bus voltage and providing the grid synchronization through the phase-locked loop (PLL) in addition, controlling the grid current as well. As accepted, the PLL block provides a nonlinear feedback control system that synchronizes its output in frequency and phase [3]. With regards to the control of other converters such as ESS converter and interlinking inverter is out of the detailed scope of the paper, it can be asserted that the cascaded-PI reference voltage-current controller structure has been preferred to achieve good performance, and also obtained sensor data for the next step with deep learning application.

III. DEEP NEURAL NETWORK-BASED SENSORLESS CONTROL APPROACH

A. DEEP NEURAL NETWORKS

AI seeks to resemble the mindset in a biological brain. The brains comprise many neurons, and these neurons are connected with biological neural networks that facilitate the

behavior process. It is utilized to train and test for the static or dynamic nonlinear relationships in any engineering problem that should be solved. AI is a large cluster that involves machine learning and deep learning subsequently, which is implemented in a variety of industry fields such as energy, automotive, textile, telecommunication, finance, nutrition, software, and agriculture, etc [36]. For deep learning structure, it can be asserted that it is formed by ANNs with many hidden layers roughly. In other words, the ANN structure has been improved to adjust wider and deeper an ANN structure easily in order to deal with the engineering problems such as regression, estimation, classification, and recognition [5].

Deep learning is an extension of neural networks, namely, it is a type of machine learning that employs multiple layers that corresponds to a DNN. It is formed by a neural network that contains two or more neural networks. The training data train the DNN using learning rules. When the network is trained, input data is provided and the network produces the output. Apart from the known ANN models, the back-propagation algorithm was invented in 1985 [40], and then the problem of training multiple layer neural networks was solved to a certain extent; however, its performance could not meet expectations on practical problems. The back-propagation is a technique to train the weights in hidden layers to obtain the optimum output [36]. Since a neural network has a quite simple architecture, it could not be improved due to its limited scope for a long time.

It is worth mentioning that we have trained the network using the back-propagation method and utilized the supervised learning-based DNN structure. For a better explanation, it can be claimed that supervised learning is like finding the correct solution that means the correct answer is already known. Additionally, the output we have got is subtracted from the correct output, so the difference between output (y_i) and correct output (d_i) is an error (e_i) of i^{th} neuron as specified by (8). A DNN stores info about the current weights, namely, to train a network with new info, we have to modify the weights. In other words, the errors are passed back to the hidden layers to adjust the weights of the nodes, thereby the correct outputs are predefined. This systematic way of modifying the weights is called "*Learning Rule*."

$$e_i = d_i - y_i, \tag{8}$$

Among the rules, the generalized delta rule is broadly preferred. Based on the errors, the weights should be adjusted using this rule as

$$w_{ij} \leftarrow w_{ij} + \Delta w_{ij}, \tag{9}$$
$$\Delta w_{ij} = \alpha \delta_i x_j, \tag{10}$$

then,

$$\delta_i = \varphi'(v_i) e_i, \tag{11}$$
$$w_{ij} \leftarrow w_{ij} + \alpha \varphi'(v_i) e_i x_j, \tag{12}$$

where, a is learning rate should be between zero and one ($0 < a < 1$), φ is derivative of the activation function, v_i represents a weighted sum of output node-i (i.e. i^{th} neuron). To sum up the back-propagation algorithm, the complete process flow can be elucidated as follows:

- **i.** Initialize the weights with proper values (kernel initializer),
- **ii.** Calculate e_i and δ_i,
- **iii.** Propagate the output node δ_i^l in the l^{th} layer, backward and forward nodes,
- **iv.** Repeat step iii till it converges the hidden layer,
- **v.** Modify the weights on the basis of the learning rule,
- **vi.** Recur steps ii-v for all training points,
- **vii.** Recur steps ii-vi till the network is trained accordingly.

By the way, the flow from step ii (including) to step vii (excluding) is called an epoch. To this end, three different technics exist such as stochastic gradient descent, batch, and mini-batch methods for the supervised learning of the neural network. In the stochastic gradient descent technic, the error is calculated for each training data and the weights are updated rapidly. In the batch technic, the error is calculated for every training data, then each weight update is calculated; however, the average value of the weight updates is used to adjust the weights in (13). Lastly, the mini-batch method involves both features from previous methods, which is like a combination of them. This method has a speed of stochastic gradient descent and stability of the batch method. The weight updates of the selected data are calculated and trained the network with the help of average weight updates [41].

$$\Delta w_{ij} = \frac{1}{N} \sum_{r=1}^{N} \Delta w_{ij}(r), \tag{13}$$

where, $\Delta w_{ij}(r)$ is the weight update for r^{th} training data, N denotes the total number of the training data.

As mentioned accordingly, deep learning has overcome multiple key developments, and the improvement of these technologies eventually formed into the current deep learning. The first impediment was training multiple layers, which was solved by a back-propagation algorithm. The second problem with deep learning was an existing poor performance. The reason for poor performance is improper training and also the reason for improper training are vanishing gradient, overfitting, and computational burden. The gradient is similar to the "Delta Learning Rule" of the back-propagation algorithm. Once the output errors do not achieve to reach the further nodes, it can be counted as a vanishing gradient [41].

In the back-propagation algorithm, the errors are passed to hidden layers to train the network. If the errors do not reach the hidden layer, the weights cannot be adjusted. That means the hidden layers cannot be trained. Thereby, there is no point in training hidden layers if they cannot be trained. This problem can be solved using the Rectified Linear Unit (ReLU) function as an activation function. This function provides us the maximum value between zero and given input. We will

need the derivative of the ReLU function to handle this issue.

$$\varphi(x) = \begin{cases} x, & x > 0 \\ 0, & x \leq 0 \end{cases} = \max(0, x), \tag{14}$$

with

$$\varphi'(x) = \begin{cases} 1, & x > 0 \\ 0, & x \leq 0 \end{cases} \tag{15}$$

To calculate the output of a certain neuron in any layer l ($1 < l < K$) of DNN structure with ReLU activation function, the output of any hidden layer are specified with a_j^{l-1} ($1 \leq j \leq N_{l-1}$), all they are then multiplied with weights w_{ij}^l from the j^{th} neuron in the $(l\text{-}1)^{th}$ layer to the i^{th} neuron in the l^{th} layer and bias terms b_i^l (for the bias of the i^{th} neuron in the l^{th} layer) are accumulated. With these notations, a_i^l of the i^{th} neuron in the l^{th} layer is associated with the activations in the $(l\text{-}1)^{th}$ layer as

$$\alpha_i^l = f_{\text{ReLU}}\left(\sum_{i=0}^{N_{l-1}} w_{ij}^l a_j^{l-1} + b_i^l\right); \quad i = 1, \ldots, N_l, \tag{16}$$

then the output for the last layer-K,

$$y_i = w_i^K a_i^k, \tag{17}$$

and also, (16) can be expressed in the vectorized form as follows:

$$\alpha^l = f_{\text{ReLU}}\left(w^l a^{l-1} + b^l\right). \tag{18}$$

Besides, DNNs are vulnerable to overfitting, as the model becomes more complicated and it involves more hidden layers. As known, the complicated models are more vulnerable to overfitting as opposed to being well-trained network like a contradiction. The most classical solution to this problem is the Dropout issue. Dropout is training some of the randomly chosen nodes rather than the whole network. For example, the first selected ones will be trained and the rest of the nodes will be set to zero for deactivating in the next training phase. Normally, half of the nodes are dropped out for hidden layers and a quarter of the nodes are dropped out for the output layer to produce acceptable results. Another effective method of preventing overfitting is regularization. It simplifies the architecture of the network as much as possible.

The last challenge of DNNs is the time required to complete the training not to cause a massive computational burden. The number of weights increases geometrically with numbers of hidden layers and more layers require more training data. A large number of training data raises the training time. Although training time is not a big deal, it is a critical issue from a practical development perspective. To finalize the training process faster, it is better to prefer higher performance hardware such as a graphical processing unit (GPU) instead of a central processing unit (CPU), the training algorithm also plays a key role such as using batch normalization

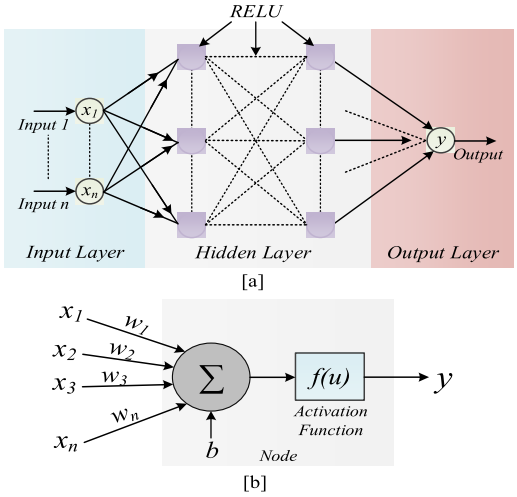

FIGURE 4. Schematic of [a] feedforward deep neural network and [b] node structure.

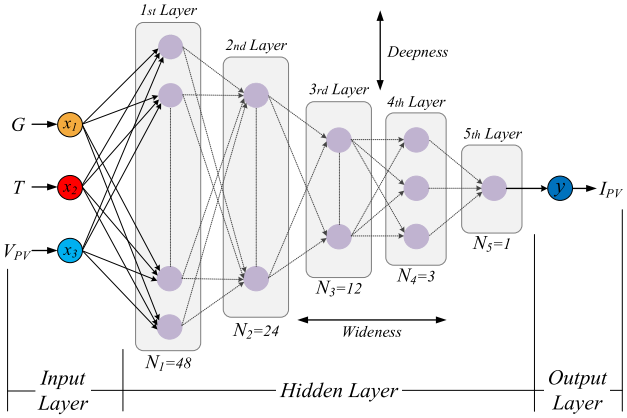

FIGURE 5. Structure of the designed DNN. Weights and bias terms are not shown in the figure to get simplicity. Inputs and outputs are highlighted with different colors, whereas the hidden layer with grey. Adjustment of getting wider structure occurs with adding more hidden layer, while deeper structure requires adding more neuron in the hidden layers.

algorithm for enhancing the performance. Upon challenging the difficulties, the weight matrices are defined for each hidden layer. The description of the proposed DNN structure is seen in Fig. 4.

B. DEPLOYMENT OF DEEP NEURAL NETWORK

Generally, it is quite meaningful to be focused on such variables that have a dynamic nonlinear relationship for estimation and regression problems [42]. This kind of relationship enables us to utilize any value that needs to be forecasted with high accuracy values. A DNN aims to mimic a sub-simulation of the biological network using electronic circuits. or more time series are utilized to estimate future values. According to the conventional equivalent circuit of PV panel, I_{PV} is stated as (20)

$$-I_{PH} + I_D + I_{SH} + I_{PV} = 0, \tag{19}$$

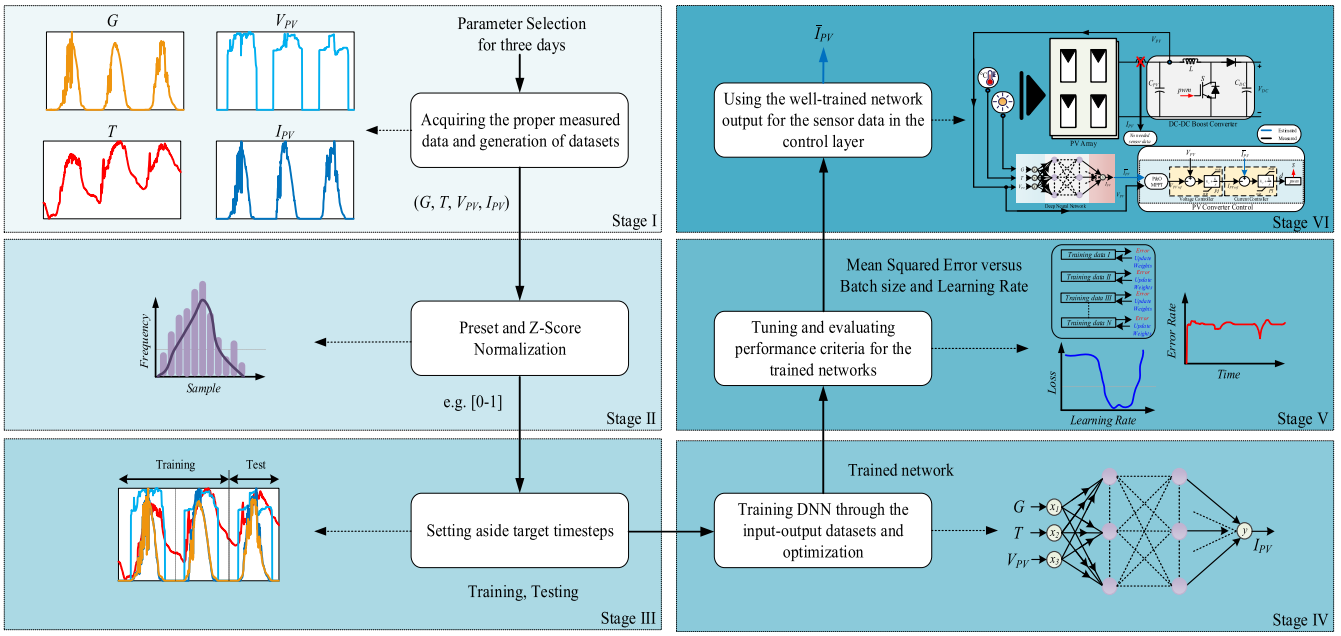

FIGURE 6. Application stages of operation of PV-Battery-based DC nanogrid with deep supervised learning in six steps.

with

$$I_{PV} = I_{PH} - I_D - I_{SH}, \tag{20}$$

$$V_t = \frac{nkT_{STC}}{q}, \tag{21}$$

$$I_{PV} = I_{PH} - I_D \left(e^{\frac{V_{CELL}+I_{PV}R_S}{nVt}} - 1\right) - \frac{V_{CELL} + I_{PV}R_S}{R_{SH}}, \tag{22}$$

where, I_D diode saturation current, R_S and R_{SH} series, and shunt resistances, respectively, and n is diode ideality factor. meteorological inputs result in a thermal cell voltage called V_t. While q identifies the electron charge, k is the Boltzmann constant. Also, the generated photocurrent-I_{PH} depends on solar irradiance (G) and temperature (T),

$$I_{PH} = I_{SC} + k_i(T - T_{stc})\frac{G}{G_{stc}}, \tag{23}$$

where, I_{SC} is short circuit current, k_i is short circuit current temperature coefficient, T_{STC} and G_{STC} respectively reference temperature and solar irradiance at standard test conditions (STC). Consequently, estimating future values of the current data-I_{PV} facilitates to be a remedy in the control layer, since sensible input-output relationship exists between G, T, V_{PV} and I_{PV}. Thereby, we have implemented a multi-layer feedforward DNN architecture in this study, which is a more complex structure than an ANN structure. Each of the hidden layers operates the information flow from the input to the output layer. Referring to the inputs of the designed DNN whilst obtaining input-memory order of past values up to delay (d) pieces of $x(t)$ is specified as a matrice of state variables:

$$x(t) = [x_1(t-1), \ldots, x_1(t-d), x_2(t-1), \ldots, x_2(t-d), x_3(t-1), \ldots, x_3(t-d)]_{nxr}, \tag{24}$$

namely,

$$x(t) = [G(t-1), \ldots, G(t-d), T(t-1), \ldots, T(t-d), V_{PV}(t-1), \ldots, V_{PV}(t-d)]_{nxr}, \tag{25}$$

thereby, the output of the model can be expressed as in (26) using with n inputs and hidden layers,

$$y(t) = [y(t-1), \ldots, y(t-d)]_{1xr}. \tag{26}$$

The proposed sensorless control scheme with DNNs can be mainly examined under six stages including proper input selection, defining the paradigms, estimation, and implementation. After completing these all stages as follows, we are ready to implement the well-trained DNN into the system as the last stage.

Stage I: After acquiring the proper data from measurements through the sensor data of the conventional cascaded-PI controlled system operation, the DNNs datasets are ready to be processed during the first stage accordingly. It is important to emphasize that we consider the total number of datasets that have equal elements.

Stage II: With the completion of the first step, the acquired data to be used for training are preset and subjected to Z-Score Normalization or Standardscaler that is a method of normalizing data to prevent outlier problems. In other words, the reason why we do apply is that; we need to compare attributes

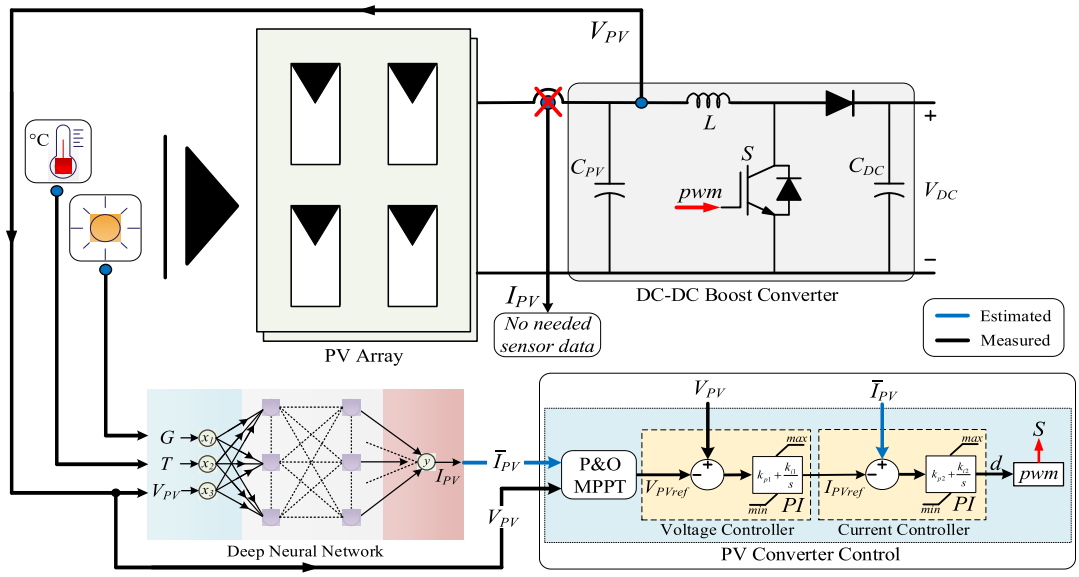

FIGURE 7. Overview of last application stage: operation of PV-Battery-based DC nanogrid with a trained DNN.

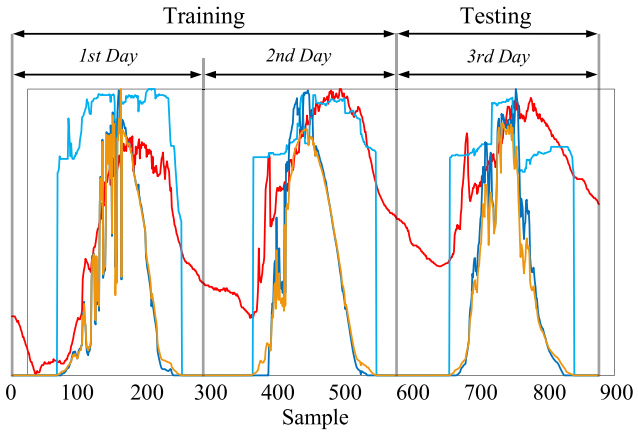

FIGURE 8. Used datasets for three days' data. The datasets are highlighted with fawn, red, aqua, and dark blue colors. Antecedent two days' data are used for training and the rest of data i.e., third day's data used for testing phase.

with very large values and attributes with small value equally. The basis z-score formula is expressed as

$$z = \frac{(x - \mu)}{\sigma}, \tag{27}$$

where, x is a test score, μ is the mean value, and lastly σ is the standard deviation of the feature. Any value is evaluated according to being equal, lower, or higher than the mean values of the feature [43].

Stage III: Input and output parameters are divided as target timestamps. Roughly, there is a query to answer such as "how many datasets will be used for the training part and test part? In order to analyze the trained network elaborately, we have divided target time steps as one-day data from three days' data and utilized two days' data for training. Then, the rest of the data i.e., the third-day data used for the testing part. In other words, the test dataset is different from the training data to provide a reliable trained DNN. If we have taken all three days' data for training, the output would encounter an overfitting problem.

Stage IV: After making a decision about the training and test datasets, DNN is trained and optimized with the aim of getting a high performance. As the latest trend optimizer, "Adam" optimizer has been preferred. This optimizer belongs to an adaptive learning rate optimization algorithm and computes on the gradient handled on the mini-batch method [44], [45].

Stage V: After the number of layers was determined, fine-tuning is performed by changing the hyper-parameters such as epoch size, learning rate, batch size, which can be adjusted for the network [32]. For network performance, the wider structure means increasing the hidden layers, while the number of neurons in the hidden layers can be increased for the deeper structure. The structure of the designed DNN is depicted in Fig. 5. To evaluate the performance criteria for the trained network, (28) expresses mean squared error (*MSE*) which is used as a loss function:

$$MSE = \frac{1}{N}\sum_{i=1}^{N} e_i^2 = \frac{1}{N}\sum_{i=1}^{N} |d_i - y_i|^2. \tag{28}$$

Hyper-parameters such as epoch size, learning rate, batch size, and neuron architecture can be adjusted according to the accuracy [46]. If the poor performance still exists, it is notable to focus on the number, type, and suitability of the used datasets.

Stage VI: By reducing the amount of *MSE* value, a well-trained network including current data can then be ready for the exploitation phase in the control layer instead of the old used one. The measured current data from the former controller is ignored and the output of the trained network is embedded into the control layer. All of these stages can

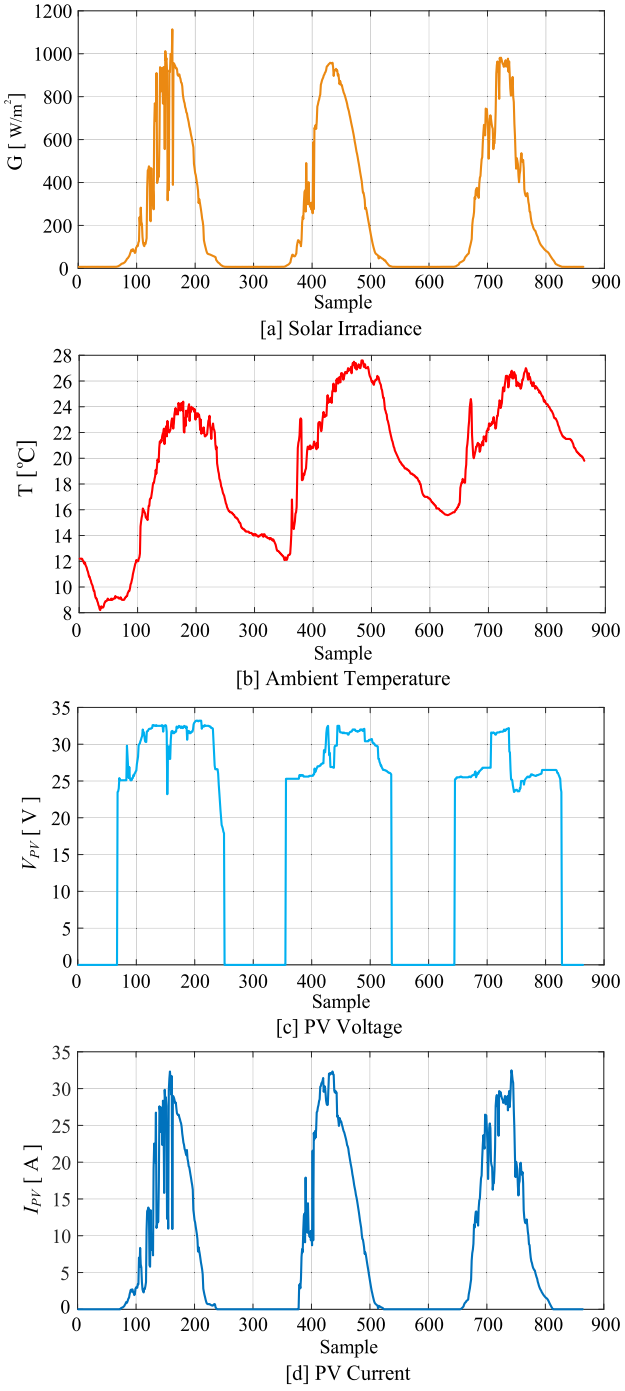

FIGURE 9. Measured data for training phase of DNNs for three days with 864 samples: [a] solar irradiance, [b] ambient temperature, [c] PV voltage-V_{PV}, and [d] PV current-I_{PV}.

be summarized in Fig. 6 and also the overview of the final application stage is shown in Fig. 7.

IV. NUMERICAL RESULTS

In this section, the proposed deep learning-aided sensorless control approach for PV Converters in DC nanogrids is implemented by considering different complications. These results validate that the proposed method represents a viable

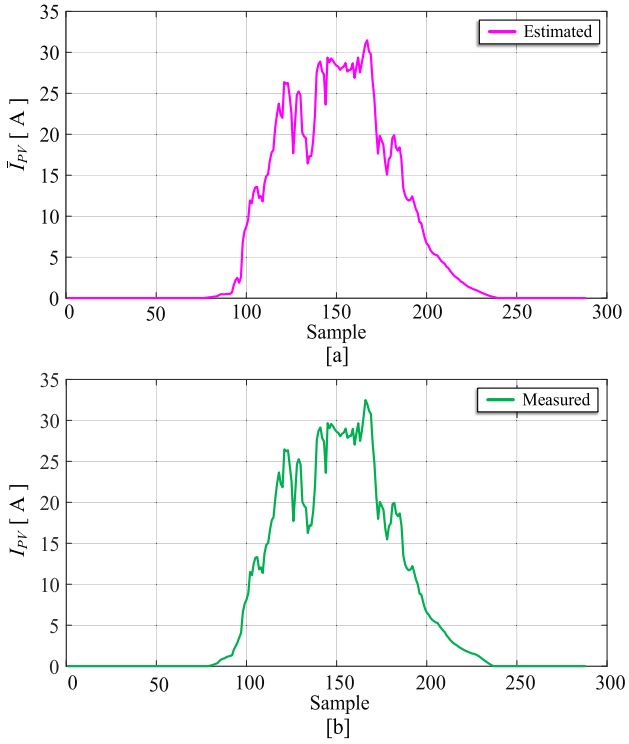

FIGURE 10. [a] Estimated and [b] measured currents for PV converter operation.

alternative to the sensorless control approach. To realize the proposed strategy's validation and efficacy, hyper-parameters of the training part were modified and tested. Also, the average value of five testing results was carried out and compared with each other.

To get high performance in a short time, the complier computer should have good features. Thus, the study results were obtained using Python-3.6 with Keras 2.3.1 TensorFlow 2.4.0 (developed by *Google*) i.e., Keras-Backend TensorFlow open-source library that is capable of parallel processing on compute unified device architecture (CUDA) graphics cards. All of the processes were operated in PyCharm software as a compiler with the help of Numpy, Pandas, and SciKit-Learn libraries. The server computer has some specifications such as a 7th generation Intel i7-7700 K processor, Nvidia GTX GeForce 1080 TI 11 gigabyte (GB) GPU, 512 GB (solid-state drive) SSD, and 1 terabyte (TB) hard disk drive (HDD).

The datasets have been measured and obtained for three days. Assuming that the weather station generates measured data per five minutes, on the grounds of a day contain twenty-four hours, we can collect the number of samples (*NoS*) per day as (24 hours $*$60 mins)/(5 mins) is equal to 288 samples. Each day comprises 288 data points, so we have performed to utilize three days' data that corresponds to 864 samples. As mentioned in the previous Section-*Stage III,* three days' data have been reserved for the training as two days' data and the testing phase as one day's data. It is considerable to distinguish the training and testing dataset from all datasets not to meet any potential performance challenges

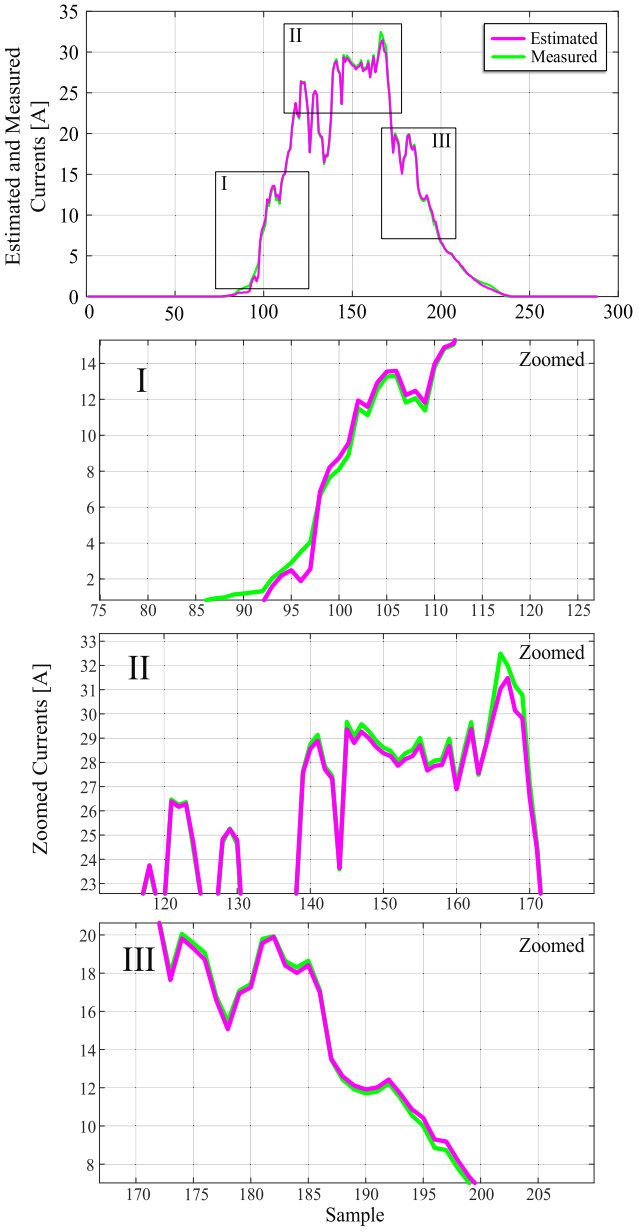

FIGURE 11. Estimated-$\dot{I}_{PV}$ and measured-I_{PV} current values.

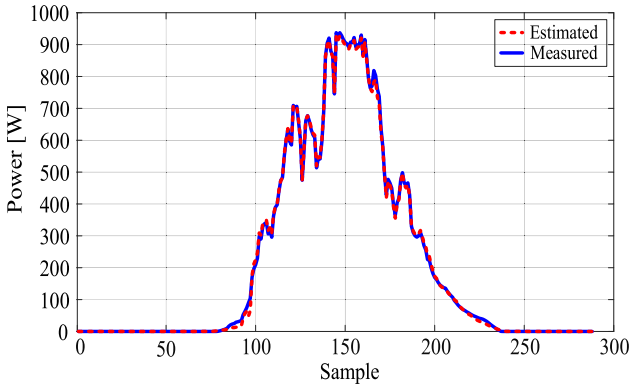

FIGURE 12. Estimated-$\dot{P}_{PV}$ and measured-P_{PV} powers regarding generated power in PV array.

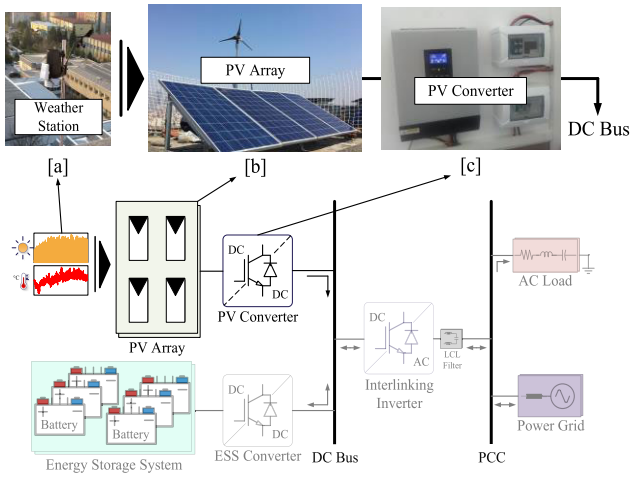

FIGURE 13. Studied experimental setup of DC nanogrid, [a] weather station, [b] PV array, [c] PV converter.

of the DNNs. Since we have distinguished the datasets, the DNNs are never tested through the training data. Accordingly, it performs on a reliable operation under different conditions like distinct input datasets. While Fig. 8 shows the whole datasets allocation for three days, the used datasets to train the DNN are seen in Fig. 9 obviously. It is important to mention that the datasets were acquired in June. As judged in Fig. 9, except for the temperature data the other sensors' data could not generate any value due to being night times. When the sunshine rises up, it is obvious that the quantitive values of the temperature, voltage, and current datasets increase as well.

As seen in Fig. 10, the estimated-$\dot{I}_{PV}$ and actual measured-I_{PV} values of PV current are shown separately. The key point is here that the estimated one is expected to converge the measured one as much as possible. Similarly, the same mentioned currents can be expressed in Fig. 11 with their zoomed points. This estimated result has been expressed by the most intimate one (i.e., with the best *MSE*) between all results.

Furthermore, estimating current data enables power estimation as well in PV systems. For power estimation, estimated and measured powers can be shown in Fig. 12. As mentioned before, the input datasets are generated with the help of the real-time operation of a real experimental setup of a DC nanogrid, which is visualized in Fig. 13. Fig. 13 (a) and (b) illustrate the weather station and PV array on the rooftop of the faculty building, while Fig. 13 (c) shows the PV converter in the laboratory. For a better illustration of the implemented method, arbitrary results with different *MSE*s (including the best one in Fig. 11) are proved to be distinct characters in Fig. 14.

All measured values are expressed with the green line. To raise the importance of implementing well-trained networks with convenient *MSE* values, different results with different quantitive *MSE*s are compared to each other in Fig. 15 with zoomed points apart from the best one

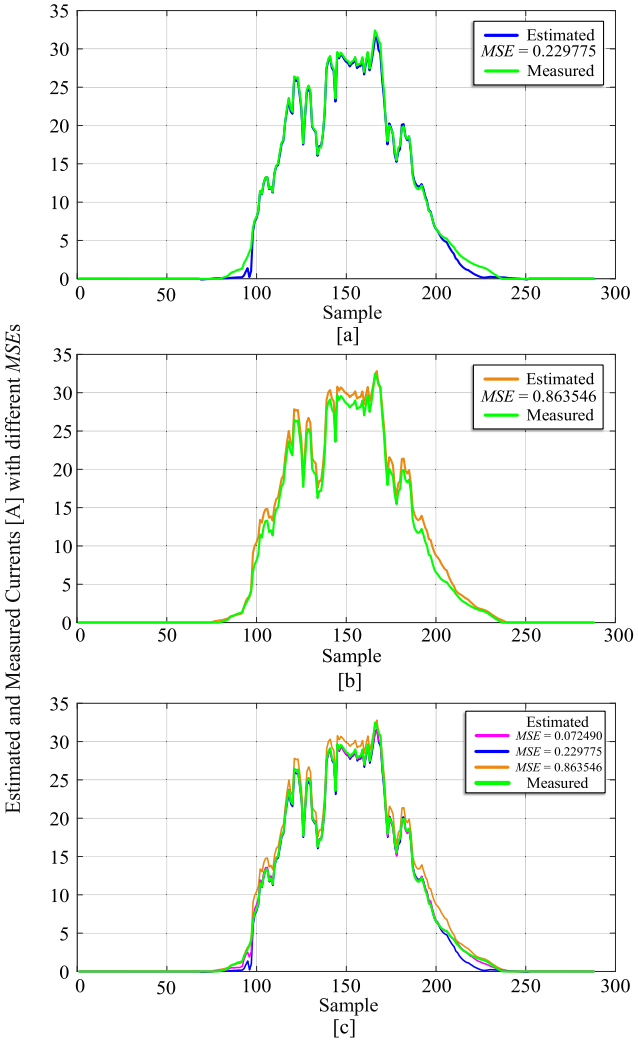

FIGURE 14. Comparison of estimated currents with the measured one. The green line expresses the measured one, while the others are all estimated ones.

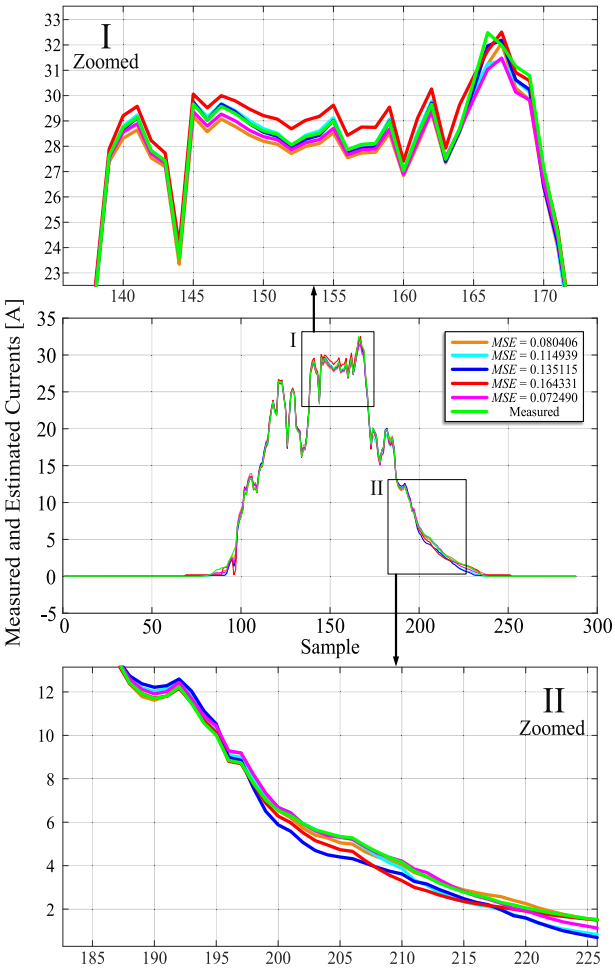

FIGURE 15. Estimated currents are compared to each other with their zoomed points. The green line expresses the measured one, while the rest of all are estimated ones.

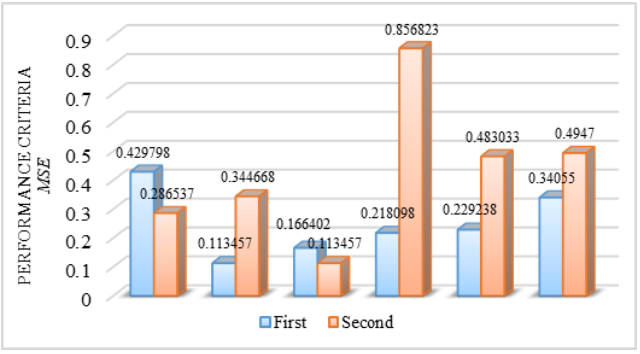

FIGURE 16. Comparison of different configurations: while the first case remarks the change of the batch size (see Table 2), the second one belongs to the chnge of learning rate (see Table 3).

(in Figs. 10 (a) and 11). It is remarkable that some of the results converge properly when the current is high as opposed to performing well when the current is low. Broadly, it is obvious that the more accuracy is achieved, the more convergence is captured and also the fewer *MSE* values are reached.

V. DISCUSSION

As stated previously, while designing the networks, the architecture can be modified having made deeper and wider structures. After assuring the final network structure, modifications of the significant hyper-parameters aid to improve the network mission such as giving more accurate output, reducing low computational burden with a fast training process.

To this end, two different configurations were proved as follows:

i) The first configuration has been prompted with a fixed epoch size equal to 1000, a learning rate equal to 0.0001, and variable batch size, as can be seen in Table 2.

On account of obtaining the best average *MSE* value with a batch size equal to 32 in this configuration, the batch size of the second configuration has been fixed as the same value as 32.

ii) The second configuration has proceeded with the same epoch size as 1000, the same batch size as 32, and variable learning rate, as can be seen in Table 3.

TABLE 2. First case results.

Features			Mean Squared Error (*MSE*)	Average Value
Epoch	Learning Rate	Batch Size		
1000	0.001	16	0.152924	0.429798
			0.217302	
			0.363000	
			0.552219	
			0.863546	
		32	0.072490	0.113457
			0.080406	
			0.114939	
			0.135115	
			0.164331	
		48	0.188958	0.166402
			0.119019	
			0.141539	
			0.152721	
			0.229775	
		96	0.168467	0.218098
			0.192820	
			0.271864	
			0.315812	
			0.141525	
		200	0.299272	0.229238
			0.188821	
			0.172609	
			0.166682	
			0.318806	
		500	0.264669	0.340550
			0.293191	
			0.438629	
			0.334757	
			0.371507	

TABLE 3. Second case results.

Features			Mean Squared Error (*MSE*)	Average Value
Epoch	Batch Size	Learning Rate		
1000	32	0.0001	0.375625	0.286537
		0.0001	0.223489	
		0.0001	0.090744	
		0.0001	0.424846	
		0.0001	0.317985	
		0.0005	0.237782	0.344668
		0.0005	0.518078	
		0.0005	0.348764	
		0.0005	0.309679	
		0.0005	0.309036	
		0.0010	0.072490	0.113457
		0.0010	0.080406	
		0.0010	0.114939	
		0.0010	0.135115	
		0.0010	0.164331	
		0.0025	1.619907	0.856823
		0.0025	2.022840	
		0.0025	0.200500	
		0.0025	0.342936	
		0.0025	0.097931	
		0.0050	1.277175	0.483033
		0.0050	0.226590	
		0.0050	0.180249	
		0.0050	0.201417	
		0.0050	0.529735	
		0.0100	0.394716	0.494700
		0.0100	0.475015	
		0.0100	0.569173	
		0.0100	0.491619	
		0.0100	0.542978	

As observed from Table 2 and 3 (and also in Fig. 16) respectively, higher batch size accomplishes slower convergence, whereas lower batch size shows non-convergence behavior with less accuracy i.e., higher error rate (see the error of the first line with a low batch size being higher than the others in Table 2). Despite being higher batch size takes less training time than being the lower batch size in the training phase.

Besides, it is extracted from Table 3 that the effect of learning rate modifications has not been generalized in parallel to the effect of batch size modifications, because the average error values show uneven characteristics according to the variable learning rate. As known, *MSE* values should be received attention to be variable due to the incalculable computational effort of DNN structure for each training.

As can be seen in the Tables, the best convergence rate was obtained epoch size equal to 1000, batch size equal FIGURE 11. Estimated-$\bar{I}_{PV}$ and measured- I_{PV} current values. to 32, and learning rate equal to 0.001 with the lowest *MSE* value as 0.072490. Additionally, Fig. 16 depicts the performance criteria-*MSE*s in terms of different configurations with the order of change of the hyper-parameters (from small to high values) as obtained in Tables 2 and 3.

VI. CONCLUSION AND FUTURE WORK

To sum up our work, it can be asserted that we have highlighted a supervised deep-learning aided control application for PV-Battery-based DC nanogrids. The findings of this paper indicate that this deep learning-based approach can tackle the system dynamics and track the PV current sensor data for the control layer properly. This paper essentially shows how the deployment of the DNN structure can support solving regression estimation problems to provide more reliable systems by eliminating the sensor data. We have also validated the effectiveness of the proposed approach once the system was trained by splitting up the training and test datasets. The strong point of our study lies in reaching high accuracy, utilizing real datasets without generating artificial data, and complying with the real application data. The proposed controller for handling regression issues with high accuracy (with an average *MSE* equal to 0.113457) and a fast response (average 29.23 secs training time) assures the usefulness of this approach. It is worth mentioning that this approach has features to be adjusted for different datasets.

This study has gone some way towards enhancing our understanding of supervised deep learning for PV-Battery-based nanogrids. In our view, these results constitute a valuable initial step towards the real-time application. Since the performance of the proposed controller has been encouraging, one promising application of our technique would be a design of a controller board that is embedded deep learning algorithm for the experimental implementation of this approach.

ACKNOWLEDGMENT

The authors would like to extend their thanks Prof. Dr. Bulent Oral and Prof. Dr. Safak Saglam for the valuable help using the weather station at Marmara University.

REFERENCES

[1] X. Fang, S. Misra, G. Xue, and D. Yang, "Smart grid—The new and improved power grid: A survey," *IEEE Commun. Surveys Tuts.*, vol. 14, no. 4, pp. 944–980, 4th Quart., 2012, doi: 10.1109/SURV.2011.101911.00087.

[2] M. Baharizadeh, H. R. Karshenas, and M. S. G. Esfahani, "Control method for improvement of power quality in single interlinking converter hybrid AC-DC microgrids," *IET Smart Grid*, vol. 4, no. 4, pp. 414–428, Aug. 2021, doi: 10.1049/stg2.12014.

[3] A. N. Akpolat, Y. Yang, F. Blaabjerg, E. Dursun, and A. E. Kuzucuoğlu, "Design implementation and operation of an education laboratory-scale microgrid," *IEEE Access*, vol. 9, pp. 57949–57966, 2021, doi: 10.1109/ACCESS.2021.3072899.

[4] K. Sun, L. Zhang, Y. Xing, and J. M. Guerrero, "A distributed control strategy based on DC bus signaling for modular photovoltaic generation systems with battery energy storage," *IEEE Trans. Power Electron.*, vol. 26, no. 10, pp. 3032–3045, Oct. 2011, doi: 10.1109/TPEL.2011.2127488.

[5] A. N. Akpolat, M. R. Habibi, E. Dursun, A. E. Kuzucuoglu, Y. Yang, T. Dragicevic, and F. Blaabjerg, "Sensorless control of DC microgrid based on artificial intelligence," *IEEE Trans. Energy Convers.*, early access, Dec. 11, 2020, doi: 10.1109/TEC.2020.3044270.

[6] D. Salomonsson, L. Söder, and A. Sannino, "Protection of low-voltage DC microgrids," *IEEE Trans. Power Del.*, vol. 24, no. 3, pp. 1045–1053, Jul. 2009, doi: 10.1109/TPWRD.2009.2016622.

[7] T. Dragičević, X. Lu, J. C. Vasquez, and J. M. Guerrero, "DC microgrids—Part I: A review of control strategies and stabilization techniques," *IEEE Trans. Power Electron.*, vol. 31, no. 7, pp. 4876–4891, Jul. 2016, doi: 10.1109/TPEL.2015.2478859.

[8] F. Nejabatkhah and Y. W. Li, "Overview of power management strategies of hybrid AC/DC microgrid," *IEEE Trans. Power Electron.*, vol. 30, no. 12, pp. 7072–7089, Dec. 2015, doi: 10.1109/TPEL.2014.2384999.

[9] A. N. Akpolat, E. Dursun, A. E. Kuzucuoğlu, Y. Yang, F. Blaabjerg, and A. F. Baba, "Performance analysis of a grid-connected rooftop solar photovoltaic system," *Electronics*, vol. 8, no. 8, p. 905, Aug. 2019, doi: 10.3390/electronics8080905.

[10] E. A. Ebrahim, N. A. Maged, N. Abdel-Rahim, and F. Bendary, "Photovoltaic-based interconnected-modified DC-nanogrids within an open energy distribution system," in *Proc. 6th Int. Conf. Adv. Control Circuits Syst. (ACCS) 5th Int. Conf. New Paradigms Electron. Inf. Technol. (PEIT)*, Hurgada, Egypt, Nov. 2019, pp. 253–258, doi: 10.1109/ACCS-PEIT48329.2019.9062843.

[11] M. R. Khan and E. D. Brown, "DC nanogrids: A low cost PV based solution for livelihood enhancement for rural Bangladesh," in *Proc. 3rd Int. Conf. Develop. Renew. Energy Technol. (ICDRET)*, Dhaka, Bangladesh, May 2014, pp. 1–5, doi: 10.1109/ICDRET.2014.6861687.

[12] D. Burmester, R. Rayudu, W. Seah, and D. Akinyele, "A review of nanogrid topologies and technologies," *Renew. Sustain. Energy Rev.*, vol. 67, pp. 760–775, Jan. 2017, doi: 10.1016/j.rser.2016.09.073.

[13] R. Haroun, A. El Aroudi, A. Cid-Pastor, E. Vidal-Idiarte, H. Valderrama-Blavi, and L. Martinez-Salamero, "Modelling and control of modular DC-nanogrids based on loss-free resistors," *IEEE Access*, vol. 8, pp. 33305–33317, 2020, doi: 10.1109/ACCESS.2020.2974036.

[14] Q. Xu, T. Dragicevic, L. Xie, and F. Blaabjerg, "Artificial intelligence-based control design for reliable virtual synchronous generators," *IEEE Trans. Power Electron.*, vol. 36, no. 8, pp. 9453–9464, Aug. 2021, doi: 10.1109/TPEL.2021.3050197.

[15] D. Zhou, G. Zhang, and F. Blaabjerg, "Optimal selection of power converter in DFIG wind turbine with enhanced system-level reliability," *IEEE Trans. Ind. Appl.*, vol. 54, no. 4, pp. 3637–3644, Jul./Aug. 2018, doi: 10.1109/TIA.2018.2822239.

[16] A. Sangwongwanich, Y. Yang, D. Sera, and F. Blaabjerg, "Mission profile-oriented control for reliability and lifetime of photovoltaic inverters," *IEEE Trans. Ind. Appl.*, vol. 56, no. 1, pp. 601–610, Jan. 2020, doi: 10.1109/TIA.2019.2947227.

[17] W. E. Aouni and L.-A. Dessaint, "Real-time implementation of input-state linearization and model predictive control for robust voltage regulation of a DC-DC boost converter," *IEEE Access*, vol. 8, pp. 192101–192108, 2020, doi: 10.1109/ACCESS.2020.3032327.

[18] X. Li, X. Zhang, F. Lin, and F. Blaabjerg, "Artificial-intelligence-based design (AI-D) for circuit parameters of power converters," *IEEE Trans. Ind. Electron.*, early access, Jun. 16, 2021, doi: 10.1109/TIE.2021.3088377.

[19] H. Farsizadeh, M. Gheisarnejad, M. Mosayebi, M. Rafiei, and M. H. Khooban, "An intelligent and fast controller for DC/DC converter feeding CPL in a DC microgrid," *IEEE Trans. Circuits Syst. II, Exp. Briefs*, vol. 67, no. 6, pp. 1104–1108, Jun. 2020, doi: 10.1109/TCSII.2019.2928814.

[20] U. Raveendrannair, M. Sandelic, A. Sangwongwanich, T. Dragicevic, R. C. Castello, and F. Blaabjerg, "An analysis of multi objective energy scheduling in PV-BESS system under prediction uncertainty," *IEEE Trans. Energy Convers.*, early access, Jan. 29, 2021, doi: 10.1109/TEC.2021.3055453.

[21] W. Dong, S. Li, X. Fu, Z. Li, M. Fairbank, and Y. Gao, "Control of a buck DC/DC converter using approximate dynamic programming and artificial neural networks," *IEEE Trans. Circuits Syst. I, Reg. Papers*, vol. 68, no. 4, pp. 1760–1768, Apr. 2021, doi: 10.1109/TCSI.2021.3053468.

[22] K. M. Sundaram, A. Hussain, P. Sanjeevikumar, J. B. Holm-Nielsen, V. K. Kaliappan, and B. K. Santhoshi, "Deep learning for fault diagnostics in bearings, insulators, PV panels, power lines, and electric vehicle applications—The state-of-the-art approaches," *IEEE Access*, vol. 9, pp. 41246–41260, 2021, doi: 10.1109/ACCESS.2021.3064360.

[23] S. Peyghami, T. Dragicevic, and F. Blaabjerg, "Intelligent long-term performance analysis in power electronics systems," *Sci. Rep.*, vol. 11, no. 1, pp. 1–18, Dec. 2021, doi: 10.1038/s41598-021-87165-3.

[24] M. R. Habibi, S. Sahoo, S. Rivera, T. Dragicevic, and F. Blaabjerg, "Decentralized coordinated cyber-attack detection and mitigation strategy in DC microgrids based on artificial neural networks," *IEEE J. Emerg. Sel. Topics Power Electron.*, early access, Jan. 11, 2021, doi: 10.1109/JESTPE.2021.3050851.

[25] M. G. M. Abdolrasol, R. Mohamed, M. A. Hannan, A. Q. Al-Shetwi, M. Mansor, and F. Blaabjerg, "Artificial neural network based particle swarm optimization for microgrid optimal energy scheduling," *IEEE Trans. Power Electron.*, early access, Apr. 22, 2021, doi: 10.1109/TPEL.2021.3074964.

[26] K. Y. Yap, C. R. Sarimuthu, and J. M.-Y. Lim, "Artificial intelligence based MPPT techniques for solar power system: A review," *J. Modern Power Syst. Clean Energy*, vol. 8, no. 6, pp. 1043–1059, 2020, doi: 10.35833/MPCE.2020.000159.

[27] D. Korkmaz, H. Acikgoz, and C. Yildiz, "A novel short-term photovoltaic power forecasting approach based on deep convolutional neural network," *Int. J. Green Energy*, vol. 18, no. 5, pp. 525–539, Apr. 2021, doi: 10.1080/15435075.2021.1875474.

[28] H. Cimen, N. Cetinkaya, J. C. Vasquez, and J. M. Guerrero, "A microgrid energy management system based on non-intrusive load monitoring via multitask learning," *IEEE Trans. Smart Grid*, vol. 12, no. 2, pp. 977–987, Mar. 2021, doi: 10.1109/TSG.2020.3027491.

[29] M. Hajihosseini, M. Andalibi, M. Gheisarnejad, H. Farsizadeh, and M.-H. Khooban, "DC/DC power converter control-based deep machine learning techniques: Real-time implementation," *IEEE Trans. Power Electron.*, vol. 35, no. 10, pp. 9971–9977, Oct. 2020, doi: 10.1109/TPEL.2020.2977765.

[30] A. Moradzadeh, H. Moayyed, S. Zakeri, B. Mohammadi-Ivatloo, and A. P. Aguiar, "Deep learning-assisted short-term load forecasting for sustainable management of energy in microgrid," *Inventions*, vol. 6, no. 1, p. 15, Feb. 2021, doi: 10.3390/inventions6010015.

[31] S. M. J. Jalali, S. Ahmadian, A. Khosravi, M. Shafie-khah, S. Nahavandi, and J. P. S. Catalao, "A novel evolutionary-based deep convolutional neural network model for intelligent load forecasting," *IEEE Trans. Ind. Informat.*, early access, Mar. 12, 2021, doi: 10.1109/TII.2021.3065718.

[32] F. Guo, B. Xu, W.-A. Zhang, C. Wen, D. Zhang, and L. Yu, "Training deep neural network for optimal power allocation in islanded microgrid systems: A distributed learning-based approach," *IEEE Trans. Neural Netw. Learn. Syst.*, early access, Feb. 10, 2021, doi: 10.1109/TNNLS.2021.3054778.

[33] *High Performance 60 Cell Poly crystalline 156×156mm Solar Photovoltaic Module*. Chinaland Solar Energy Co., Ltd. Accessed: 2020. [Online]. [Online]. Available: https://westech-pv.com/download/250Watt.pdf

[34] A. Sangwongwanich, Y. Yang, F. Blaabjerg, and H. Wang, "Benchmarking of constant power generation strategies for single-phase grid-connected photovoltaic systems," *IEEE Ind. Appl. Mag.*, vol. 54, no. 1, pp. 447–457, Jan./Feb. 2018, doi: 10.1109/TIA.2017.2740380.

[35] C. Albea, A. Sferlazza, F. Gordillo, and F. Gomez-Estern, "Control of power converters with hybrid affine models and pulse-width modulated inputs," *IEEE Trans. Circuits Syst. I, Reg. Papers*, vol. 68, no. 8, pp. 3485–3494, Aug. 2021, doi: 10.1109/TCSI.2021.3083900.

[36] A. N. Akpolat, E. Dursun, and A. E. Kuzucuoglu, "AI-aided control of a power converter in wind energy conversion system," in *Proc. Innov. Intell. Syst. Appl. Conf. (ASYU)*, Oct. 2020, pp. 1–6, doi: 10.1109/ASYU50717.2020.9259877.
[37] P. K. Pardhi, S. K. Sharma, and A. Chandra, "Control of single-phase solar photovoltaic supply system," *IEEE Trans. Ind. Appl.*, vol. 56, no. 6, pp. 7132–7144, Nov. 2020, doi: 10.1109/TIA.2020.3024171.
[38] M. Fekri, N. Molavi, E. Adib, and H. Farzanehfard, "High voltage gain interleaved DC–DC converter with minimum current ripple," *IET Power Electron.*, vol. 10, no. 14, pp. 1924–1931, Nov. 2017, doi: 10.1049/iet-pel.2016.0675.
[39] D. Czarkowski, L. R. Pujara, and M. K. Kazimierczuk, "Robust stability of state-feedback control of PWM DC-DC push-pull converter," *IEEE Trans. Ind. Electron.*, vol. 42, no. 1, pp. 108–111, Feb. 1995, doi: 10.1109/41.345854.
[40] D. E. Rumelhart and J. L. McClelland, "Learning internal representations by error propagation," in *Parallel Distributed Processing: Explorations in the Microstructure of Cognition: Foundations*, Cambridge, MA, USA: MIT Press, 1987, pp. 318–362.
[41] P. Kim, *MATLAB Deep Learning: With Machine Learning, Neural Networks and Artificial Intelligence*. New York, NY, USA: Apress, 2017, doi: 10.1007/978-1-4842-2845-6.
[42] B. Adineh, M. R. Habibi, A. N. Akpolat, and F. Blaabjerg, "Sensorless voltage estimation for total harmonic distortion calculation using artificial neural networks in microgrids," *IEEE Trans. Circuits Syst. II, Exp. Briefs*, vol. 68, no. 7, pp. 2583–2587, Jul. 2021, doi: 10.1109/TCSII.2021.3059410.
[43] Code Academy. (2021). *Z-Score Normalization*. [Online]. Available: https://www.codecademy.com/articles/normalization
[44] Towards Data Science. (2021). *Adam-Latest Trends in Deep Learning Optimization*. [Online]. Available: https://towardsdatascience.com/adam-latest-trends-in-deep-learning-optimization-6be9a291375c
[45] D. P. Kingma and J. Ba, "Adam: A method for stochastic optimization," 2014, *arXiv:1412.6980*. [Online]. Available: https://arxiv.org/abs/1412.6980
[46] A. Iranfar, M. Zapater, and D. Atienza, "Multi-agent reinforcement learning for hyperparameter optimization of convolutional neural networks," *IEEE Trans. Comput.-Aided Design Integr. Circuits Syst.*, early access, May 3, 2021, doi: 10.1109/TCAD.2021.3077193.

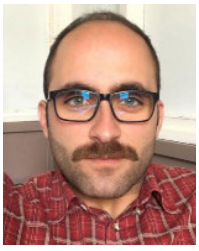

ALPER NABI AKPOLAT (Member, IEEE) received the B.Sc. degree in electrical-electronics engineering and the M.Sc. degree in mechatronics engineering from Firat University, Elâzığ, Turkey, in 2012 and 2015, respectively. He is currently pursuing the Ph.D. degree in electrical-electronics engineering with the Faculty of Technology, Marmara University, Istanbul, Turkey.

Since March 2019, he has been a Guest Ph.D. Student with the Department of Energy Technology, Aalborg University, Denmark, for one year. He is currently serving as a Research Assistant with the Faculty of Technology, Marmara University. His research interests include renewable energy systems, DC microgrids, applied artificial intelligence in power electronics and power systems, and control of distributed generation systems.

ERKAN DURSUN (Member, IEEE) received the B.Sc., M.Sc., and Ph.D. degrees in electric education from the Faculty of Technical Education, Marmara University, Istanbul, Turkey, in 2001, 2006, and 2013, respectively.

From 2010 to 2012, he was a Visiting Fellow with the United Nations Industrial Development Organization–International Centre for Hydrogen Energy Technologies (UNIDO-ICHET). From 2012 to 2013, he was a Researcher with the Joint Research Center, European Commission, Italy. His articles have received more than 520 citations in SCI database of Thomson Reuters. His research interests include distributed generation, hybrid power systems, and smart grid.

AHMET EMIN KUZUCUOĞLU (Member, IEEE) received the B.Sc. degree from the Department of Electronics and Telecommunication Engineering, Istanbul Technical University, Istanbul, Turkey, in 1985, and the M.Sc. and Ph.D. degrees from Marmara University, Istanbul, in 1994 and 2000, respectively.

He has been the part of YÖK-World Bank Vocational School Project, England and USA, in 1987. He has been the part of EU Leonardo da Vinci Type A mobility Project, Lithuania, in July 2006. Since 2017, he has been serving as the Vice Dean of the Faculty of Technology, Marmara University, where he is currently an Associate Professor with the Department of Electrical-Electronics Engineering. His current research interests include industrial automation, robotics, AI, and control theory and applications. He is the Editor-in-Chief of *International Periodical of Recent Technologies in Applied Engineering* (PORTA).